

Phononic Weyl Nodal Straight Lines in High-Temperature Superconductor MgB_2

Qing Xie^{‡,1,2} Jiangxu Li^{‡,1,3} Min Liu,^{1,3} Lei Wang,^{1,3} Dianzhong Li,¹ Yiyi Li,¹ and Xing-Qiu Chen^{1,*}

¹Shenyang National Laboratory for Materials Science, Institute of Metal Research,
Chinese Academy of Sciences, Shenyang 110016, China

²University of Chinese Academy of Sciences, Beijing 100049, China

³School of Materials Science and Engineering, University of Science and Technology of China, 110016 Shenyang, Liaoning, China

(Dated: October 5, 2021)

Based on first-principles calculations, we predict that the superconducting MgB_2 with a AlB_2 -type centrosymmetric lattice host the so-called phononic topological Weyl nodal lines (PTWNLs) on its bulk phonon spectrum. These PTWNLs can be viewed as countless Weyl points (WPs) closely aligned along the straight lines in the $-\text{H-K-H}$ direction within the three-dimensional Brillouin zone (BZ). Their topological non-trivial natures are confirmed by the calculated Berry curvature distributions on the planes perpendicular to these lines. These lines are highly unique, because they exactly locate at the high-symmetry boundary of the BZ protected by the mirror symmetry and, simultaneously, straightly transverse the whole BZ, in different from known classifications including nodal rings, nodal chains or nets, and nodal loops. On the $(10\bar{1}0)$ crystal surface, the PTWNLs-induced drumhead-like non-trivial surface states appear within the rectangular area confined by the projected lines of the PTWNLs with opposite chirality. Moreover, when the mirror symmetry is broken, the double-degenerate PTWNLs are further lifted to form a pair WPs with opposite chirality. Our results pave the ways for future experimental study on topological phonons on MgB_2 and highlights similar results in a series of isostructural AlB_2 -type metallic diborides.

As accompanying with extensive studies of topological insulators, topological semimetals and even topological superconductors in their electronic structures[1–3], topological phonons [4–8] have been most recently attracted attentions in condensed matter physics and material sciences. This is mainly because the topological phononic states will be interesting for potential applications. In different from various electronic fermions, phonons, as one of bosons, are not limited by the Pauli exclusion principle. This fact demonstrates that the whole frequency zone of phonon spectrum can be physically probed. In similarity to topological properties of electrons, the topological effects of phonons can induce the one-way edge phonon states or topologically protected surface phononic states. Physically, these states will conduct phonon with little or no scattering[4, 5], suggesting possible applications for designing phononic circuits[6]. For instance, utilizing the one-way edge phonon states an ideal phonon diode [6] was proposed with a fully 100% efficiency in a multi-terminal transport system. It was even theoretically uncovered that the chirality of topological phonons excited by polarized photons can be detected by a valley phonon Hall effect in monolayer hexagonal lattices [8]. In particular, it needs to be emphasized that in similarity to various fermions of electrons, the exciting progresses of the bosons (vibrational phonons) have been also predicted [7] or observed in the 3D momentum space of solid crystals with the topological vibrational states, such as Dirac, Weyl and line-node phonons in photonic crystals with macroscopic acoustic systems of kHz frequency [4, 5, 7, 9–21] and theoretically predicted doubly-Weyl phonons in transition-metal monosilicides with atomic vibrations at THz frequency [22]. Most recently, also in a series of WC-type family of materials (i.e., ZrS, ZrSe and ZrTe) with atomic vibration at THz frequency, the single topological Weyl phonons are predicted and they exist opening topological arcs of surface phonons, connecting pairs of surface-

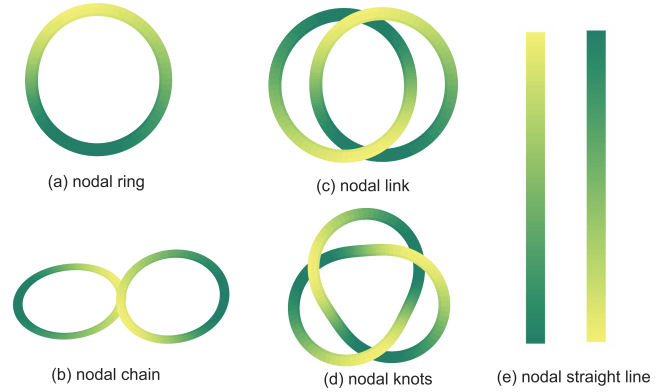


FIG. 1. Known main classifications of topological nodal lines: (a) isolated nodal ring, (b) nodal chain, (c) nodal link, (d) nodal knot, and (e) nodal straight lines extending the whole BZ in an one-way direction.

projected Weyl points with opposite chirality[23]. However, to date no phononic topological Weyl nodal lines have been reported in macroscopic acoustic systems at kHz frequency or in atomic vibrational periodic lattices at THz frequency.

It needs to be emphasized that topological nodal lines [24] have been already and extensively studied in electronic band structures, optical lattices, photonic and acoustic systems. It has been found that symmetries, i.e., both \mathcal{P} and \mathcal{T} ones, can protect the presence of various nodal lines. Once these symmetries are broken, nodal lines would be gapped out or form Dirac points (DPs) or WPs. To date, nodal lines have been classified into various categories, such as (i) isolated closed nodal rings (Fig. 1(a)) in alkaline earth metals of hcp Be and Mg [25], of fcc Ca and Sr [25, 26], TiSi-family [27], 3D carbon allotropes [28], antiperovskite $\text{Cu}_3(\text{Pb,Zn})\text{N}$ [29, 30], Ca_3P_2 [31], photonic crystals [7], and a hyperhoneycomb

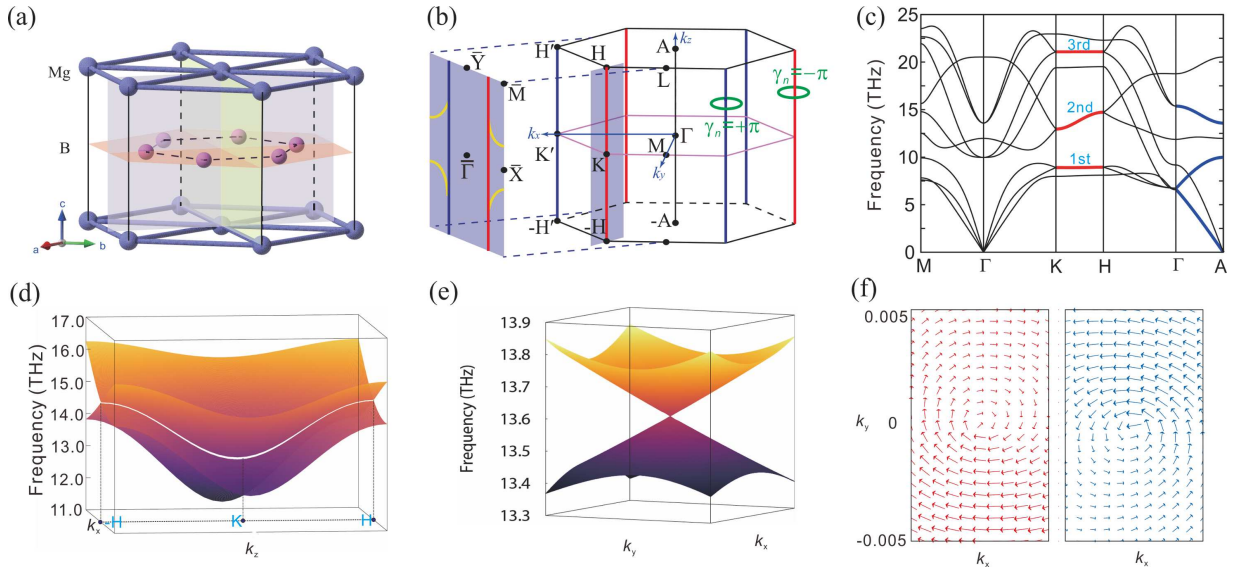


FIG. 2. (a) Crystal structure of MgB_2 . Three shadowed planes are the mirror planes. (b) The Brillouin zone and $(10\bar{1}0)$ surface. The PTWNLs transverse the whole BZ along both the $-H$ to H and the $-H'$ to H' directions. Red (blue) lines have negative (positive) chirality. Each PTWNL extends through the whole BZ 1 times along one of the direction and carries a topological charge $Q = \gamma_n/\pi = \pm 1$ using the input of the Berry phase. The surface states at about 14.2 THz are schematically depicted on the surface. (c) The phonon dispersion of MgB_2 along the high-symmetry momentums paths in the BZ. Three red thick bands (as marked by the 1st, 2nd, and 3rd) along the H-K direction correspond to double-degenerate PTWNLs, whereas three blue thick double-generate bands along the Γ -A direction are topologically trivial. (d) Three-dimensional phononic bands around the 2nd PTWNL on the shaded k -plane across the $-H$ -K- H direction as shown in the 3D BZ in the panel (b). (e) Three-dimensional phononic bands at any WP on any PTWNL. Here, we visualize it by selecting a node on the 2nd PTWNL at $k_z = 0.2$. (f) Berry curvature distributions on the xy plane around two nodal points of the 2nd PTWNLs at $(1/3, 1/3, 0.2)$ and $(-1/3, 2/3, 0.2)$, respectively.

lattice [32], (ii) nodal chain or nodal net (Fig. 1(b)) in which several closed nodal rings touch at a point to form a chain (or a net) stretching in the whole BZ of both iridium tetrafluoride [33], HfC [34], graphene network structure [35] and TiS[23], (iii) nodal link (Fig. 1(c)) featured with closed nodal loops which are linked and intertwined with each other in so-called Hopf link semimetal Co_2MnGa [36] and (iv) nodal knots (Fig. 1(d)) in which a nodal ring entangles with itself to form nodal knot structure [37]. Besides these four main types of nodal lines structures, some discontinuous nodal lines can also exist in BZ, such as in monoclinic C_{16} [38] and metallic rutile oxides [39]. To date, no Weyl nodal *straight* lines (Fig. 1(f)) have been reported in various materials.

Within this context, through first-principles calculations, we report that the famous high-temperature BCS-type superconductor[40, 41], MgB_2 , hosts the phononic topological Weyl nodal lines (PTWNLs) in its bulk BZ of the phonon spectrum. MgB_2 has a AlB_2 -type hexagonal lattice [42] in a space group of $P6/mmm$ (No. 191) in Fig. 2(a). Mg at the Wyckoff site $1a$ $(0,0,0)$ and B occupying the $2d$ $(\frac{1}{3}, \frac{2}{3}, \frac{1}{2})$ site form two-dimensional triangular and honeycomb lattices, respectively. Two layers interleaved along z -axis. Based on symmetry analysis, it has been noted that there are three double-degenerate phonon bands along the directions from $-H(\frac{1}{3}, \frac{1}{3}, -\frac{1}{2})$ to $H(\frac{1}{3}, \frac{1}{3}, \frac{1}{2})$ in the bulk BZ as illustrated in Fig. 2(b). The calculations demonstrate that these double-

degenerate phonon bands exactly are PTWNLs. The Berry phases of the defined loops around these PTWNLs are derived to be $\pm\pi$, indicating their non-trivial topological nature. Berry curvature distributions uncover their chirality. In addition, on the $(10\bar{1}0)$ surface, we observe PTWNLs-induced drumhead-like non-trivial surface states, which are indeed very similar with the topological surface states found in topological Dirac nodal line systems. When the inversion symmetry is broken, the double-degenerate PTWNLs can be further lifted up and WPs can be formed. Afterwards, the surface states form opening Fermi arc structure connecting these WPs. In addition, we have noted that the other three doubly-degenerate phononic bands form $-A(0, 0, -\frac{1}{2})$ to $A(0, 0, \frac{1}{2})$ in the bulk BZ are topologically trivial, without appearance of any phononic topological surface states.

Methods.— We perform first-principles calculations based on density functional theory (DFT) [53, 54] with generalized gradient approximation (GGA) in the form of Perdew-Burke-Ernzerhof function [55, 56] for exchange-correlation potential. The calculations are performed using the Vienna *ab initio* simulation package (VASP) [51, 52]. A self-consistent field method (tolerance 10^{-5} eV/atom) is employed in conjunction with planewave basis sets of cutoff energy of 500 eV. Atomic structure optimization is implemented until the remanent Hellmann-Feynman forces on the ions are less than 0.001 eV/Å. We use a Γ -centered $11 \times 11 \times 17$ k point mesh

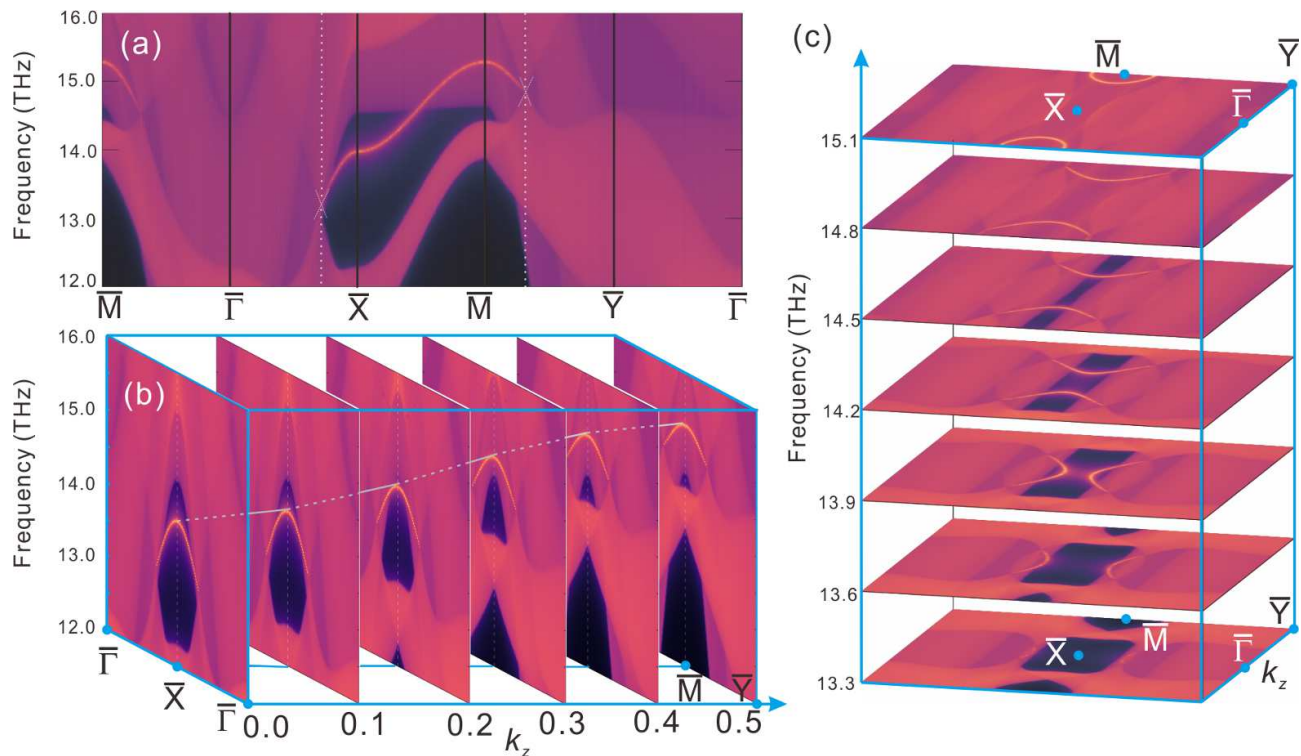


FIG. 3. Phononic states on the $(10\bar{1}0)$ surface of MgB_2 . (a) The surface phonon spectrum along high symmetry lines. (b) The evolution of the surface phonon spectra and the topologically protected phononic non-trivial surface states by increasing the k_z value along the $\bar{\Gamma} - \bar{X} - \bar{\Gamma}$ direction. (c) The frequency-dependent evolution of the phononic surface states of the $(10\bar{1}0)$ BZ as defined in Fig. 2(b) to show the change of the phononic drumhead non-trivial surface states in the rectangular region confined by the projected lines of two PTWNLs with opposite chirality.

to sample the BZ. Phonon spectra are obtained using the density functional perturbation theory (DFPT) with a Born-Karman boundary condition implemented in the Phonopy package [57]. The force constants are calculated using a $3 \times 3 \times 3$ supercell and are taken as the tight-binding parameters to build the dynamic matrices. The surface DOS are obtained by using the iteration Green's function method [59].

Structure.— The optimized lattice constants are $a = 3.074 \text{ \AA}$ and $c = 3.513 \text{ \AA}$. These values are in good agreements with previous experimental [40–42] and computational [43–47] results. The structure is shown in Fig. 2(a).

Phonon spectra.— Figure 2(c) presents the phonon spectrum of MgB_2 along high symmetry momentum paths, which are in nice agreement with previous calculations [43–47] and experimental characterizations [48–50]. At the high-symmetry $K(\frac{1}{3}, \frac{1}{3}, 0)$ and $H(\frac{1}{3}, \frac{1}{3}, \frac{1}{2})$ points, there are three double-degenerate points each. Phonon spectrum along $-H$ to H in Fig. 2(c) evidences the existence of the three double-degeneracy bands, which are PTWNLs in the strictly *straight* lines traversing the whole BZ. In Figs. 2(d) and 2(e), we depicted the phonon dispersions along a PTWNL on the xz -plane and around a specified point, $(1/3, 1/3, 0.2)$ in a unit of reciprocal lattice vector, of a PTWNL on the xy -plane. It can be seen that their dispersion around any point of the PTWNLs exhibits a linear dispersion on the xy -plane. It is a hallmark

of a WP. In other words, these 1st, 2nd, and 3rd PTWNLs in Fig. 2(c) are highly unique. In the first, they along the $-H-K-H$ direction can be viewed as countless WPs closely aligned in the straight lines in its three-dimensional BZ. In the second, each PTWNL can extend through the whole BZ along this high-symmetry direction in the momentum space. In particular, all of them exactly lie at the BZ boundary along the one-way high-symmetry direction, which are indeed protected by the mirror symmetry. In addition, it needs to be emphasized that, although such Dirac-line behaviors stretching the whole BZ along the one direction has been recently outlined in the electronic structures of rhombohedrally stacked honeycomb lattices [60] and of nanostructured carbon allotropes [61], these symmetry-protected PTWNLs along the one-direction high-symmetry lines in the phonon spectrum of MgB_2 is still recognized for the first time. Mechanically, these three different PTWNLs are associated with three distinct phonon modes. The 1st PTWNL mainly involves the in-plane vibrational mode of Mg atoms, the 2nd one is totally determined by the out-of-plane vibrational mode of two boron atoms moving in opposite or same directions along the c axis while the Mg is stationary, and the 3rd one only involves the in-plane motion in which boron moves along the x or y axes and Mg along almost the diagonal direction of the xy axes. Another difference for these three PTWNLs is that the 2nd

PTWNL shows an apparent k -dependent dispersion of the frequencies, whereas both the 1st and 3rd PTWNLs are nearly flat in the frequencies against k vector along the $-H$ - K - H or $-H'$ - K' - H' directions as shown in Fig. 2(c).

Topological properties of phonon.— To determine the topological nature of these PTWNLs, we have derived the corresponding Berry phases and Berry curvature distributions. For a closed loop in 3D BZ, the berry phase is defined as

$$\gamma_n = \oint_C \mathbf{A}_n(\mathbf{k}) \cdot d\mathbf{l}, \quad (1)$$

where $\mathbf{A}_n(\mathbf{k}) = i\langle u_n(\mathbf{k}) | \nabla_{\mathbf{k}} | u_n(\mathbf{k}) \rangle$ is the Berry connection and $u_n(\mathbf{k})$ is the Bloch wavefunction of n -th band. As illustrated in Fig. 2(b), we have first selected a closed circle on the xy -plane centered at a momentum position of the PTWNL (see the circle marked by the green curves). Note that the radius of the closed circles going around each PTWNL can be selected to be arbitrary large, as long as it does not also cover another PTWNL. Interestingly, we have found that their Berry phase for all three PTWNLs along the $-H$ - K - H direction are π , whereas the other three PTWNLs along the $-H'$ - K' - H' direction have an opposite Berry phase of $-\pi$. This means that these PTWNLs are topological non-trivial and it also proves that the topological nature of the PTWNLs along the $-H$ - K - H direction and $-H'$ - K' - H' direction are opposite in their chirality. As a further supporting evidence, we can directly visualize the source or sink effects by deriving the Berry curvature distributions, $\Omega_n(\mathbf{k}) = \nabla \times \mathbf{A}_n(\mathbf{k})$, on the xy -plane, as shown in Figure 2(f).

In addition, as shown in the phonon spectrum from Γ to A in Fig. 2(c) there are also three two-fold degenerate lines. However, the analysis of their Berry phases and Berry curvatures confirm that these three lines are indeed topological trivial. Their associated vibrational phonon modes were already discussed in a previous publication [47].

Phononic drumhead-like surface states.— Furthermore, we have identified the surface phonon spectrum of the $(10\bar{1}0)$ surface of MgB_2 . As expected, there should have topologically protected phononic non-trivial drumhead-like surface states in the rectangular region confined by the projected lines of the PTWNLs along the K to H direction and along the K' to H' direction. We calculate surface phononic density of states (PDOSs) by using the iteration Green's function method [59]. After Fourier transforming the force constants, surface Green's function is built from dynamical matrix and the surface DOS is taken from the imaginary part of surface Green's function. Figure 3 presents the surface states on the MgB_2 $(10\bar{1}0)$ surface. In Fig. 3(a), we depict the surface PDOSs along high symmetry moment paths on the surface BZ ranging from 12.0 THz to 16.0 THz to clearly show the phononic surface states associated with the 2nd PTWNL. It can be seen in Fig. 3 that in the \bar{X} - \bar{M} direction the bright phononic non-trivial surface states are clearly observable. In Figs. 3(b) and 3(c), we further show the evolutions of drumhead-like surface states with respect to increasing k_z and frequency, respectively. We observe that the surface

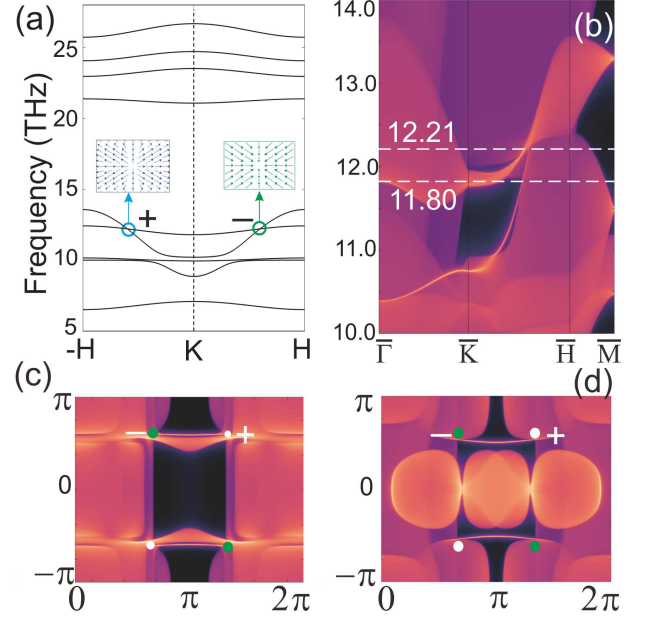


FIG. 4. Phonon dispersion along the $-H$ - K - H direction of the artificial MgBC and its $(10\bar{1}0)$ surface phonon dispersion. (a) The phonon spectra along high symmetry $-H$ - K - H line. Two WPs are observable with opposite chirality, $+$ and $-$, as illustrated by Berry curvature distributions in the insets. (b) The surface phonon spectrum along the high-symmetry lines in the $(10\bar{1}0)$ surface BZ to show the non-trivial surface states. Two dashed lines denote the frequencies of 11.80 THz and 12.21 THz, respectively. Opening arc states connecting a pair WPs with opposite chirality in (c) the surface Fermi-like plot with the frequency of 12.21 THz and (d) the surface Fermi-like plot with the frequency of 11.80 THz.

states are confined well in the rectangular region outlined by the projected lines of two 2nd PTWNLs with opposite chirality. In Fig. 3(b), with increasing k_z the downward parabolic-shape non-trivial surface states climb up to a higher frequency and the depth of the parabola becomes smaller and smaller. At $k_z = 0.5$ in Fig. 3(b), the shallow parabolic non-trivial surface state is completely above the surface state at $k_z = 0.0$. This leads to an interesting evolution of the phononic non-trivial surface states as the frequency increases. We have observed three typical types of non-trivial surface states associated with the 2nd PTWNL in Fig. 3(c). When the frequency $13.3 \lesssim f \lesssim 13.9$ THz, the surface states look like to connect two points on the same projected line of the bulk PTWNL. When $13.9 \lesssim f \lesssim 14.8$ THz, the surface states clearly connect two points on the two projected lines of the bulk PTWNLs with opposite chirality. When $14.8 \lesssim f \lesssim 15.1$ THz, the surface states form a ring on the 2D surface BZ and do not intersect with any projected lines of the bulk PTWNLs. Indeed, in another two different frequency regions below 12 THz or above 16 THz, we can certainly observe the phononic non-trivial surface states which are associated with the 1st and 3rd PTWNLs along the bulk K - H directions.

Phononic Weyl points and surface arcs.— Interestingly, our calculations also reveal that the double degeneracy of these

PTWNLs can be lifted, possibly resulting in the appearance of WPs, when both the mirror and inversion symmetries are broken. To elucidate this feature, we have substituted one boron atom with a carbon atom in the MgB_2 unit cell, leading to the composition of MgBC . With such a treatment, the MgBC structure now belongs to the space group of $P\bar{6}m3$ (No. 187) because the inversion symmetry is broken and, simultaneously, the mirror symmetry of the K-H direction is also broken. As illustrated in Fig. 4(a), the derived phonon dispersion along the H to K direction does not exhibit any PTWNLs due to the lifting up of double degeneracy. In contrast, a pair WPs appear because of the phonon band crossings. We also analyzed their topological nature using the Berry curvature distributions around each WP, obtaining the nonzero topological charges of ± 1 as shown in Fig. 4(a). Additionally, on the $(10\bar{1}0)$ surface we have clearly observed the opening phononic surface arc states connecting to such a pair WPs with opposite chirality in Fig. 4(b,c and d).

Finally, we have found that a series of metallic diborides, which are isostructural to MgB_2 in the AlB_2 family, host similar PTWNLs in their phonon spectra. These materials include the prototype material AlB_2 , BeB_2 , CaB_2 , CuB_2 , NaB_2 , OsB_2 , ScB_2 , SrB_2 , TaB_2 , TiB_2 , YB_2 and ZrB_2 . For each of them, there are three double-degenerate PTWNLs along $-\text{H}$ to H in the 3D BZ. These PTWNLs transverse the whole BZ and act as source or sink of the Berry curvatures. On their $(10\bar{1}0)$ crystal surface, we observed drumhead-like non-trivial phononic surface states. At certain frequencies, the drumhead-like surface states form isolated arc structures and should serve as clear signature for experimental verifications. Available experimental techniques [62–65] to probe these states include neutron scattering, electron energy loss spectroscopy and X-ray thermal diffuse scattering.

Note added.— During the preparation of this work, we became aware of a very recent manuscript proposing the electronic topological Dirac nodal lines in MgB_2 through first-principles calculations [66].

Acknowledgements Work was supported by the National Science Fund for Distinguished Young Scholars (No. 51725103), by the National Natural Science Foundation of China (Grant Nos. 51671193 and 51474202), and by the Science Challenging Project No. TZ2016004. All calculations have been performed on the high-performance computational cluster in the Shenyang National University Science and Technology Park and the National Supercomputing Center in Guangzhou (TH-2 system) with special program for applied research of the NSFC-Guangdong Joint Fund (the second phase) under Grant No.U1501501.

‡ These authors contributed equally to this work.

* xingqiu.chen@imr.ac.cn

[1] C. L. Kane and E. J. Mele, *Z₂ Topological Order and the Quantum Spin Hall Effect*, *Phys. Rev. Lett.* **95**, 146802 (2005).

- [2] M. Z. Hasan and C. L. Kane, *Colloquium: Topological insulators*, *Rev. Mod. Phys.* **82**, 3045 (2010).
- [3] Xiao-Liang Qi and Shou-Cheng Zhang, *Topological insulators and superconductors*, *Rev. Mod. Phys.* **83**, 1057 (2011).
- [4] S. H. Mousavi, A. B. Khanikaev, and Z. Wang *Topologically protected elastic waves in phononic metamaterials*, *Nat. Commun.* **6**, 8682 (2015).
- [5] C. He, X. Ni, H. Ge, X.-C. Sun, Y.-B. Chen, M.-H. Lu, X.-P. Liu, and Y.-F. Chen, *Acoustic topological insulator and robust one-way sound transport*, *Nature Phys.* **12**, 1124 (2016).
- [6] Y. Z. Liu, Y. Xu, S.-C. Zhang, and W. H. Duan, *Model for topological phononics and phonon diode*, *Phys. Rev. B* **96**, 064106 (2017).
- [7] L. Lu, L. Fu, J. D. Joannopoulos, and M. Soljačić, *Weyl points and line nodes in gyroid photonic crystals*, *Nature Photon.* **7**, 294 (2013).
- [8] L. Zhang, and Q. Niu *Chiral Phonons at High-Symmetry Points in Monolayer Hexagonal Lattices*, *Phys. Rev. Lett.* **115**, 115502 (2015).
- [9] D. Z. Rocklin, B. G. Chen, M. Falk, V. Vitelli, and T. C. Lubensky, *Mechanical Weyl Modes in Topological Maxwell Lattices*, *Phys. Rev. Lett.* **116**, 135503 (2016).
- [10] L. Lu, Z. Wang, D. Ye, L. Ran, L. Fu, J. D. Joannopoulos, M. Soljačić, *Experimental observation of Weyl points*, *Science*. **349**, 622 (2015).
- [11] S. D. Huber, *Topological mechanics*, *Nature Phys.* **12**, 621 (2016).
- [12] R. Fleury, A. B. Khanikaev, and A. Alù, *Floquet topological insulators for sound*, *Nat. Commun.* **7**, 11744 (2016).
- [13] E. Prodan, and C. Prodan, *Topological phonon modes and their role in dynamic instability of microtubules*, *Phys. Rev. Lett.* **103**, 248101 (2009).
- [14] B. G. Chen, N. Upadhyaya, and V. Vitelli, *Nonlinear conduction via solitons in a topological mechanical insulator*, *Proc Natl Acad Sci.* **111**, 13004 (2014).
- [15] Z. J. Yang, F. Gao, X. H. Shi, X. Lin, Z. Gao, Y. D. Chong, and B. L. Zhang, *Topological Acoustics*, *Phys. Rev. Lett.* **114**, 114301 (2015).
- [16] P. Wang, L. Lu, and K. Bertoldi, *Topological Phononic Crystals with One-Way Elastic Edge Waves*, *Phys. Rev. Lett.* **115**, 104302 (2015).
- [17] M. Xiao, W.-J. Chen, W. Y. He, and C. T. Chan, *Synthetic gauge flux and Weyl points in acoustic systems*, *Nature Phys.* **11**, 920 (2015).
- [18] L. M. Nasha, D. Kleckner, A. Reada, V. Vitellib, A. M. Turner, and W. T. M. Irvine, *Topological mechanics of gyroscopic metamaterials*, *Proc Natl Acad Sci.* **112**, 14495 (2015).
- [19] R. Süssstrunk, and S. D. Huber, *Observation of phononic helical edge states in a mechanical topological insulator*, *Science*. **349**, 47 (2015).
- [20] R. Süssstrunk, and S. D. Huber, *Classification of topological phonons in linear mechanical metamaterials*, *Proc Natl Acad Sci.* **113**, E4767 (2016).
- [21] F. Li, X. Huang, J. Lu, J. Ma, and Z. Liu, *Weyl points and Fermi arcs in a chiral phononic crystal*, *Nature Physics* DOI: 10.1038/NPYS42675 (2017).
- [22] T. T. Zhang, Z. D. Song, A. Alexandradinata, H. M. Weng, C. Fang, L. Lu, and Z. Fang, *Double-Weyl phonons in transition-metal monosilicides*, *Phys. Rev. Lett.*, **120**, 016401 (2018).
- [23] J.X. Li, Q. Xie, S. Ullah, R.H. Li, H. Ma, D.Z. Li, Y.Y. Li, and Xing-Qiu Chen, *Coexisted Three-component Bosons and Two-component Weyl Bosons in TiS, ZrSe and HfTe*, *arXiv:1711.09037*.
- [24] C. Fang, H. M. Weng, X. Dai, and Z. Fang, Topological nodal

- line semimetals, *Chin. Phys. B* **25**, 117106 (2016).
- [25] R.H. Li, H. Ma, X. Y. Cheng, S. L. Wang, D. Z. Li, Z. Y. Zhang, Y. Y. Li, and X.-Q. Chen *Dirac Node Lines in Pure Alkali Earth Metals*, *Phys. Rev. Lett.* **117**, 096401 (2016).
- [26] M. Hirayama, R. Okugawa, T. Miyake, and S. Murakami, *Topological Dirac nodal lines and surface charges in fcc alkaline earth metals*, *Nature Commun.* **8**, 14022 (2017)
- [27] J. X. Li, H. Ma, Q. Xie, S. B. Feng, S. Ullah, R. H. Li, J. H. Dong, D. Z. Li, Y. Y. Li, and X.-Q. Chen, *Topological quantum catalyst: Dirac nodal line states and a potential electrocatalyst of hydrogen evolution in the TiSi family*, *Sci China Mater.* **61**, 23–29, (2018)
- [28] H. M. Weng, Y. Y. Liang, Q. N. Xu, R. Yu, Z. Fang, X. Dai, and Y. Kawazoe, *Topological node-line semimetal in three-dimensional graphene networks*, *Phys. Rev. B* **92**, 045108 (2015).
- [29] R. Yu, H. M. Weng, Z. Fang, X. Dai, and X. Hu *Topological Node-Line Semimetal and Dirac Semimetal State in Antiperovskite Cu_3PdN* , *Phys. Rev. Lett.* **115**, 036807 (2015).
- [30] Y. Kim, B. J. Wieder, C. L. Kane, and A. M. Rappe *Dirac Line Nodes in Inversion-Symmetric Crystals*, *Phys. Rev. Lett.* **115**, 036806 (2015).
- [31] L. S. Xie, L. M. Schoop, E. M. Seibel, Q. D. Gibson, W. W. Xie, and R. J. Cava, *Line of Dirac Nodes in Hyperhoneycomb Lattices*, *APL Mater.* **3**, 083602 (2015).
- [32] K. Mullen, B. Uchoa, and D. T. Glatzhofer *Line of Dirac Nodes in Hyperhoneycomb Lattices*, *Phys. Rev. Lett.* **115**, 026403 (2015).
- [33] T. Bzdušek, Q. S. Wu, A. Rüegg, M. Sigrist, and A. A. Soluyanov *Nodal-chain metals*, *Nature*. **538**, 75 (2016)
- [34] R. Yu, Q. S. Wu, Z. Fang, and H. M. Weng, *From Nodal Chain Semimetal to Weyl Semimetal in HfC*, *Phys. Rev. Lett.* **119**, 036401 (2017).
- [35] J.-T. Wang, S.M. Nie, H.M. Weng, Y. Kawazoe, and C.F. Chen, *Topological nodal net semimetal in a Graphene network structure* *Phys. Rev. Lett.* in press, (2018).
- [36] G. Q. Chang, S.-Y. Xu, X. T. Zhou, S.-M. Huang, B. Singh, B. K. Wang, I. Belopolski, J. X. Yin, S. T. Zhang, and A. Bansil, H. Lin, and M. Z. Hasan, *Topological Hopf and Chain Link Semimetal States and Their Application to Co_2MnGa* , *Phys. Rev. Lett.* **119**, 156401 (2017).
- [37] R. Bi, Z. B. Yan, L. Lu, and Z. Wang, *Nodal-knot semimetals*, *Phys. Rev. B* **96**, 201305(R) (2017).
- [38] X. Feng, Q. S. Wu, Y. Cheng, B. Wen, Q. Wang, Y. Kawazoe, p. Jena, *Monoclinic C_{16} : sp^2 - sp^3 hybridized nodal-line semimetal protected by PT -symmetry*, *Carbon* **127**, 527 (2018).
- [39] Y. Sun, Y. Zhang, C.-X. Liu, C. Felser, and B. H. Yan, *Dirac nodal lines and induced spin Hall effect in metallic rutile oxides*, *Phys. Rev. B* **95**, 235104 (2017).
- [40] J. Nagamatsu, N. Nakagawa, T. Muranaka, Y. Zenitani, and J. Akimisu, *Superconductivity at 39 K in magnesium diboride*, *Nature*. **410**, 63 (2001).
- [41] D. G. Hinks, H. Claus, and J. D. Jorgensen, *The complex nature of superconductivity in MgB_2 as revealed by the reduced total isotope effect*, *Nature*. **411**, 457 (2001).
- [42] M. Jones, and R. Marsh, *The Preparation and Structure of Magnesium Boride, MgB_2* , *J. Am. Chem. Soc.*, **76**, 1434 (1954).
- [43] N. I. Medvedeva, A. L. Ivanoskii, J. E. Medvedeva, and A. J. Freeman, *Electronic structure of superconducting MgB_2 and related binary and ternary borides*, *Phys. Rev. B* **64**, 020502(R) (2001).
- [44] M. J. Mehl, D. A. Papaconstantopoulos, and D. J. Singh, *Effects of C, Cu, and Be substitutions in superconducting MgB_2* , *Phys. Rev. B* **64**, 140509(R) (2001).
- [45] N. D. Markovskiy, J. A. Muñoz, M. S. Lucas, C. W. Li, O. Delaire, M. B. Stone, D. L. Abernathy, and B. Fultz, *Nonharmonic phonons in MgB_2 at elevated temperatures*, *Phys. Rev. B* **83**, 174301(R) (2011).
- [46] P. P. Singh, *Role of Boron p-Electrons and Holes in Superconducting MgB_2 , and Other Diborides: A Fully Relaxed, Full-Potential Electronic Structure Study*, *Phys. Rev. Lett.* **87**, 087004 (2001).
- [47] T. Yildirim, O. Gülseren, J. W. Lynn, C. M. Brown, T. J. Udovic, Q. Huang, N. Rogado, K. A. Regan, M. A. Hayward, J. S. Slusky, T. He, M. K. Haas, P. Khalifah, K. Inumaru, and R. J. Cava *Giant Anharmonicity and Non-linear Electron-Phonon Coupling in MgB_2 : A Combined First-Principles Calculation and Neutron Scattering Study*, *Phys. Rev. Lett.* **87**, 037001 (2001).
- [48] A. Q.R. Baron, H. Uchiyama, S. Tsutsui, Y. Tanaka, D. Ishikawa, John P. Sutter, S. Lee c, S. Tajima, R. Heid, K.-P. Bohnen, *Phonon spectra in pure and carbon doped MgB_2 by inelastic X-ray scattering*, *Physica C* **456**, 83–91 (2008).
- [49] A. Q. R. Baron, H. Uchiyama, Y. Tanaka, S. Tsutsui, D. Ishikawa, S. Lee, R. Heid, K.-P. Bohnen, S. Tajima, and T. Ishikawa, *Kohn Anomaly in MgB_2 by Inelastic X-Ray Scattering*, *Phys. Rev. Lett.* **92**, 197004 (2004).
- [50] Abhay Shukla, Matteo Calandra, Matteo diAstuto, Michele Lazzeri, Francesco Mauri, Christophe Bellin, Michael Krisch, J. Karpinski, S. M. Kazakov, J. Jun, D. Daghero, and K. Parlinski, *Phonon Dispersion and Lifetimes in MgB_2* , *Phys. Rev. B*, **90**, 095506 (2003).
- [51] G. Kresse, and J. Hafner *Ab initio molecular dynamics for liquid metals*, *Phys. Rev. B* **47**, 558 (1993).
- [52] G. Kresse, and J. Furthmüller *Efficiency of ab-initio total energy calculations for metals and semiconductors using a plane-wave basis set*, *Comput. Mater. Sci.* **6**, 15 (1996).
- [53] P. Hohenberg and W. Kohn *Inhomogeneous Electron Gas*, *Phys. Rev.* **136**, B864 (1964).
- [54] W. Kohn and L. J. Sham *Self-Consistent Equations Including Exchange and Correlation Effects*, *Phys. Rev.* **140**, A1133 (1965).
- [55] P. E. Blöchl *Projector augmented-wave method*, *Phys. Rev. B* **50**, 17953 (1994).
- [56] J. P. Perdew, K. Burke, and M. Ernzerhof *Generalized Gradient Approximation Made Simple*, *Phys. Rev. Lett.* **77**, 17953 (1996).
- [57] A. Togo, F. Oba, and I. Tanaka, *First-principles calculations of the ferroelastic transition between rutile-type and $CaCl_2$ -type SiO_2 at high pressures*, *Phys. Rev. B* **78**, 134106 (2008).
- [58] S. Baroni, S. Gironcoli, A. D. Corso, and P. Giannozzi *Phonons and related crystal properties from density-functional perturbation theory*, *Rev. Mod. Phys.* **73**, 515 (2001).
- [59] M. P. Lopez Sancho, J. M. Lopez Sancho, J. M. L. Sancho, and J. Rubio, *Highly convergent schemes for the calculation of bulk and surface Green functions*, *Journal of Physics F: Metal Physics* **15**, 851 (1985).
- [60] T. Hyart, R. Ojaärvi, and T.T. Heikkilä, *Two topologically distinct Dirac-line semimetal phases and topological phase transitions in rhombohedrally stacked honeycomb lattices* *Arxiv: 1709.05265* (2017).
- [61] Y. P. Chen, Y. Xie, S. A. Yang, H. Pan, F. Zhang, M. L. Cohen, and S. B. Zhang, *Nanostructured Carbon Allotropes with Weyl-like Loops and Points*, *Nano Lett.* **15**, 6974 (2015).
- [62] A. Eichler, K.-P. Bohnen, W. Reichardt, and J. Hafner, *Phonon dispersion relation in rhodium: Ab initio calculations and neutron-scattering investigations*, *Phys. Rev. B* **57**, 324 (1998).

- [63] H. Ibach, *Surface vibrational studies with electron energy-loss spectroscopy*, *J. Vac. Sci. Technol. A* **5**, 419 (1987).
- [64] H. Lourenço-Martins and M. Kociak *Vibrational Surface Electron-Energy-Loss Spectroscopy Probes Confined Surface-Phonon Modes*, *Phys. Rev. X* **7**, 041059 (2017).
- [65] Ruqing Xu and Tai C. Chiang, *Determination of phonon dispersion relations by X-ray thermal diffuse scattering*, *Z. Kristallogr.* **220**, 1009 (2005).
- [66] K.-H. Jin, H. Q. Huang, J.-W. Mei, Z. Liu, L.-K. Lim, and F. Liu *Topological Dirac-Nodal-Line Semimetal Phase in High-Temperature Superconductor MgB₂*, [arxiv:1710.06996](https://arxiv.org/abs/1710.06996).